

PREX and CREX: Evidence for Strong Isovector Spin-Orbit Interaction

Tong-Gang Yue,¹ Zhen Zhang,^{2,*} and Lie-Wen Chen^{1,†}

¹*School of Physics and Astronomy, Shanghai Key Laboratory for Particle Physics and Cosmology,
and Key Laboratory for Particle Astrophysics and Cosmology (MOE),
Shanghai Jiao Tong University, Shanghai 200240, China*

²*Sino-French Institute of Nuclear Engineering and Technology, Sun Yat-sen University, Zhuhai 519082, China*
(Dated: June 7, 2024)

The recent PREX-2 and CREX data on the model-independent extraction of the charge-weak form factor difference ΔF_{CW} in ^{208}Pb and ^{48}Ca challenge modern nuclear energy density functionals (EDFs) as well as our present understanding on the neutron skin and nuclear symmetry energy. Within the Skyrme-like EDFs, we demonstrate that the isovector spin-orbit interaction can strongly change the ΔF_{CW} in ^{48}Ca while it has essentially no influence on the ΔF_{CW} in ^{208}Pb , mainly due to the eight spin-orbit unpaired $1f_{7/2}$ neutrons in ^{48}Ca . To simultaneously describe PREX-2 and CREX data in 1σ error, we find the strength of isovector spin-orbit interaction should be larger than about four times of that in the conventional Skyrme-like EDFs, implying the neutrons and protons have significantly different spin-orbit interaction. To further reconcile the data on electric dipole polarizability in ^{208}Pb and ^{48}Ca , we obtain $L \approx 55$ MeV for the slope parameter of the symmetry energy, $\Delta r_{\text{np}}(^{208}\text{Pb}) \approx 0.19$ fm and $\Delta r_{\text{np}}(^{48}\text{Ca}) \approx 0.12$ fm for the neutron skin thickness. The implications of the strong isovector spin-orbit interaction are discussed.

Introduction.—With the parity-violating elastic scattering of polarized electrons, the PREX-2 [1] and CREX [2] Collaborations recently reported model-independent determination of the charge-weak form factor difference $\Delta F_{\text{CW}}(q) \equiv F_{\text{C}}(q) - F_{\text{W}}(q)$ in ^{208}Pb and ^{48}Ca , i.e., $\Delta F_{\text{CW}}^{208} = 0.041 \pm 0.013$ and $\Delta F_{\text{CW}}^{48} = 0.0277 \pm 0.0055$ at a momentum transfer of $q = 0.3977$ fm⁻¹ and 0.8733 fm⁻¹ [2], respectively. These results have been highly anticipated, especially because the ΔF_{CW} is strongly correlated with the neutron skin thickness $\Delta r_{\text{np}} \equiv r_n - r_p$ [$r_{n(p)}$ is the point neutron(proton) rms radius of the nucleus] and thus provides an ideal probe of the density slope parameter L of nuclear symmetry energy $E_{\text{sym}}(\rho)$ [3–19], which encodes the isospin dependence of nuclear matter equation of state (EOS) and plays a crucial role in many topics of nuclear physics and astrophysics [20–31]. However, analyses of the PREX-2 and CREX results using various modern nuclear energy density functionals (EDFs) lead to conflicting conclusions on the extraction of L and Δr_{np} , with PREX-2 favoring huge L and Δr_{np} while CREX giving very small ones [2, 32–34], referred to as PREX-CREX puzzle.

A number of theoretical attempts have been devoted to understanding the PREX-CREX puzzle [32–42], and the conclusion is that the common nuclear EDFs cannot simultaneously reproduce the PREX-2 and CREX results on the ΔF_{CW} within 1σ error. Although efforts have been made very recently to reconcile the PREX-2 and CREX results within the relativistic mean field (RMF) model by including the isovector-scalar δ meson [43] and its coupling to scalar meson as well as tensor coupling [44], the solution of the PREX-CREX puzzle remains an ongoing challenge. This makes our present understanding on Δr_{np} and $E_{\text{sym}}(\rho)$ become rather elusive.

It is clear that ^{208}Pb and ^{48}Ca have different shell

structures. In particular, compared to ^{208}Pb which has 12 spin-orbit (SO) unpaired $1h_{11/2}$ protons and 14 unpaired $1i_{13/2}$ neutrons, ^{48}Ca has 8 unpaired $1f_{7/2}$ neutrons without unpaired protons, implying that the isospin-sensitive $\Delta F_{\text{CW}}^{48}$ may depend on the state-dependent isovector spin-orbit (IVSO) interaction. Note the SO interaction is also more important for lighter nuclei due to the relatively more diffused surface. It is interesting to note that the Δr_{np} of ^{48}Ca depends on the total SO interaction but that of ^{208}Pb does not [45]. In addition, the SO contribution to the electroweak skin in ^{48}Ca is significant compared to the tiny one in ^{208}Pb [46]. These observations suggest that the IVSO interaction might be the key to the PREX-CREX puzzle. It is well-known that the strong SO interaction is of fundamental importance for nuclear structure, e.g., it is responsible for nuclear magic numbers [47, 48]. While the strong SO coupling naturally emerges in the relativistic models [49, 50], nonrelativistic nuclear models such as Skyrme [51] and Gogny [52] EDFs incorporate the SO coupling via a phenomenological way. Although the isoscalar SO interaction is relatively well determined by analyzing properties of finite nuclei, the IVSO interaction is poorly known due to the lack of effective experimental probes and the complex interplay of the SO interaction with, e.g., tensor forces and nucleon effective masses [53–55].

In this Letter, within the Skyrme-like EDFs, we demonstrate that the IVSO interaction can significantly affect the $\Delta F_{\text{CW}}^{48}$ while it has negligible influence on the $\Delta F_{\text{CW}}^{208}$, and a strong IVSO interaction with its strength larger than about four times of that in the conventional Skyrme-like EDFs can solve the PREX-CREX puzzle.

Model and method.—In the present work, we use non-relativistic nuclear EDFs based on the standard (see, e.g., Ref. [56]) and extended (see, e.g., Ref. [57]) Skyrme in-

interactions. The standard Skyrme interaction has nine adjustable parameters: $t_0, t_1, t_2, t_3, x_0, x_1, x_2, x_3$ and α , which can be expressed analytically in terms of nine macroscopic quantities, including the saturation density ρ_0 , the binding energy per nucleon of symmetric nuclear matter (SNM) $E_0(\rho_0)$, the incompressibility K_0 , the magnitude $E_{\text{sym}}(\rho_0)$ and density slope L of $E_{\text{sym}}(\rho)$ at ρ_0 , the isoscalar effective mass $m_{s,0}^*$ and isovector effective mass $m_{v,0}^*$ at ρ_0 , the gradient coefficient G_S , and the symmetry-gradient coefficient G_V [45, 58, 59]. For the extended Skyrme interaction, there are six additional parameters $t_4, t_5, x_4, x_5, \beta$ and γ to mimic the momentum-dependent many-body forces. For simplicity, the values β and γ are fixed to be unit in this work. Similar to the standard Skyrme EDF, the 13 parameters of $t_0 \sim t_5, x_0 \sim x_5$ and α can be determined by 13 macroscopic quantities with four additional ones [60]: the cross gradient coefficient G_{SV} , the Landau parameter G'_0 , the skewness coefficient J_0 of SNM and the density curvature parameter K_{sym} of the $E_{\text{sym}}(\rho)$. By expressing the Skyrme parameters in terms of the macroscopic quantities, the empirical knowledge on the latter can then largely help to tune the parameters of Skyrme-like EDFs.

In the (extended) Skyrme EDFs, we further include the zero-range tensor force [61] and the SO interaction by taking the IVSO strength as a free parameter [62, 63]. The single-nucleon SO potential W_q then contains contributions from the two-body SO interaction, the central-exchange force and the tensor force, i.e.,

$$W_q = \frac{b_{\text{IS}}}{2} \nabla \rho + t_q \frac{b_{\text{IV}}}{2} \nabla (\rho_n - \rho_p) + \frac{\alpha_J + \beta_J}{2} \mathbf{J} + t_q \frac{\alpha_J - \beta_J}{2} (\mathbf{J}_n - \mathbf{J}_p), \quad (1)$$

where $t_q = 1(-1)$ for $q = n(p)$, $\rho = \rho_n + \rho_p$ with $\rho_{n(p)}$ being neutron (proton) number density, $\mathbf{J} = \mathbf{J}_n + \mathbf{J}_p$ with $\mathbf{J}_{n(p)}$ being neutron (proton) SO density, b_{IS} and b_{IV} are respectively the isoscalar and isovector SO coupling parameters. The parameters $\alpha_J = \alpha_C + \alpha_T$ and $\beta_J = \beta_C + \beta_T$ contain both central-exchange (α_C and β_C) and tensor (α_T and β_T) contributions, where α_C and β_C are determined by the Skyrme parameters while α_T and β_T are adjustable tensor-force parameters. See Supplemental Material for the detailed expressions of tensor force and the central-exchange terms.

We note that the b_{IV} is usually much less than b_{IS} in normal nuclear EDFs. In the conventional Skyrme-like EDFs, the neutron SO potential from the zero-range two-body SO interaction is $\frac{1}{2}W_0(\nabla\rho + \nabla\rho_n)$ [51, 56] with W_0 being the SO strength parameter, and this corresponds to $b_{\text{IV}} = b_{\text{IS}}/3 = W_0/2$. The nonrelativistic reduction of standard RMF models generally leads to $b_{\text{IV}} \approx 0$ [62–66].

Since we focus on doubly closed-shell nuclei in the present work, pairing correlation is neglected. Consequently, the standard Skyrme EDF has 13 adjustable model parameters: $\rho_0, E_0(\rho_0), K_0, E_{\text{sym}}(\rho_0), L, G_S$

$G_V, m_{s,0}^*, m_{v,0}^*, b_{\text{IS}}, b_{\text{IV}}, \alpha_T$ and β_T , while the extended Skyrme EDF includes additional four parameters: G_{SV}, G'_0, J_0 and K_{sym} . New EDFs are then constructed by randomly sampling in the parameter space and comparing their predictions with experimental data.

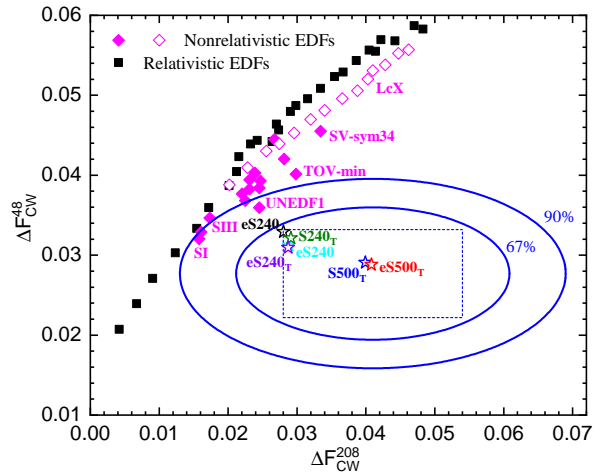


FIG. 1. The $\Delta F_{\text{CW}}^{208}$ and $\Delta F_{\text{CW}}^{48}$ from various covariant (squares) and nonrelativistic (solid diamonds [2] and open diamonds [67]) EDFs together with the 6 new Skyrme-like EDFs constructed in the present work (open stars). The ellipses depict the joint PREX-2 and CREX 67% and 90% probability contours, while the rectangle indicates the marginal 68.3% confidence intervals ($\Delta F_{\text{CW}}^{48} = 0.0277 \pm 0.0055$ and $\Delta F_{\text{CW}}^{208} = 0.041 \pm 0.013$) [2].

Results and discussions.— We begin by comparing in Fig. 1 the predictions on $\Delta F_{\text{CW}}^{48}$ and $\Delta F_{\text{CW}}^{208}$ from various modern nonrelativistic and relativistic nuclear EDFs [2, 67] with the PREX-2 and CREX results. One clearly sees that to simultaneously describe the PREX-2 and CREX results is a challenge for modern nuclear EDFs. Also included in Fig. 1 are the predictions from six new (extended) Skyrme EDFs, i.e., S240, eS240, S240_T, eS240_T, S500_T and eS500_T, constructed in the present work by using a strong IVSO interaction (see Tab. I and discussions below). Remarkably, with the inclusion of a strong IVSO interaction, all the six new EDFs can simultaneously reproduce the PREX-2 and CREX results within 1σ error, and well describe the ground state properties (e.g., masses, charge radii and spin-orbit splittings) of a number of typical (semi-)closed-shell nuclei (see Supplemental Material for the details).

Among the six new EDFs, the S500_T and eS500_T, corresponding respectively to the standard and extended Skyrme EDFs with a strong IVSO coupling of $b_{\text{IV}} = 500 \text{ MeV} \cdot \text{fm}^5$, almost perfectly reproduce the PREX-2 and CREX results. Notably, the S500_T and eS500_T predict very stiff $E_{\text{sym}}(\rho)$ with $L = 99.7 \text{ MeV}$ and 80.6 MeV , respectively, consistent with previous analyses of PREX-2 data [43, 67]. Due to the stiff $E_{\text{sym}}(\rho)$, however, the constrained Hartree-Fock calculations [68] with (e)S500_T

TABLE I. The values of interaction parameters, the predicted nuclear matter properties as well as ΔF_{CW} , Δr_{np} (fm) and α_{D} (fm³) in ²⁰⁸Pb and ⁴⁸Ca, for the six EDFs S240, eS240, S240_T, eS240_T, S500_T and eS500_T. The parameters $t_0 \sim t_2$, b_{IS} , b_{IV} , α_{T} and β_{T} are given in MeV · fm³. The t_3 , t_4 and t_5 are in units of MeV · fm^{3+3 α} , MeV · fm^{5+3 β} , and MeV · fm^{5+3 γ} , respectively. The ρ_0 is in fm⁻³, and the $E_0(\rho_0)$, $S_0 \equiv E_{\text{sym}}(\rho_0)$, L and K_{sym} are in MeV. The isoscalar and isovector effective masses are given, respectively, by $\bar{m}_{s,0} = m_{s,0}^*/m$ and $\bar{m}_{v,0} = m_{v,0}^*/m$ with nucleon mass $m = 939$ MeV.

	S240	eS240	S240 _T	eS240 _T	S500 _T	eS500 _T
t_0	-2029.4	-1777.4	-2013.2	-1707.4	-1942.9	-1632.7
t_1	319.969	534.945	312.255	576.127	310.4	545.566
t_2	328.400	-44.585	-11.507	128.93	604.89	-946.38
t_3	13713.8	12882.5	13652.8	12107.0	13579.5	12807.8
t_4	-	-1608.5	-	-1718.0	-	-1815.3
t_5	-	-1983.3	-	-1921.9	-	7734.2
x_0	0.2655	0.3706	0.2808	0.3077	-0.4972	-0.1312
x_1	-1.3375	-0.7830	-0.8068	-0.8494	-0.5167	0.8692
x_2	-1.9532	6.6536	18.785	-3.8262	-1.6533	-0.9003
x_3	0.1038	0.3573	0.1579	0.2180	-1.4670	-0.9644
x_4	-	-1.6562	-	-1.7790	-	1.6947
x_5	-	-1.8112	-	-1.8660	-	-1.1009
α	0.27317	0.35737	0.27604	0.37750	0.29794	0.43201
β	-	1	-	1	-	1
γ	-	1	-	1	-	1
b_{IS}	160.81	149.72	123.18	124.78	100.56	118.87
b_{IV}	240	240	240	240	500	500
α_{T}	0	0	-200.163	-132.004	-121.47	-1.6178
β_{T}	0	0	-51.2445	-32.56077	-295.74	-244.841
ρ_0	0.16359	0.15580	0.16498	0.15442	0.16342	0.15089
E_0	-16.147	-16.170	-16.220	-16.190	-16.288	-15.957
$\bar{m}_{s,0}$	0.982	0.939	0.993	0.865	1.022	0.921
$\bar{m}_{v,0}$	0.816	0.898	0.883	0.765	0.602	0.662
S_0	34.08	34.45	35.19	34.06	39.03	36.96
L	46.6	60.5	52.7	57.4	99.7	80.6
K_{sym}	-207.4	-87.3	-190.4	-133.1	-101.1	-189.5
$\Delta F_{\text{CW}}^{208}$	0.0280	0.0288	0.0291	0.0287	0.0400	0.0408
$\Delta F_{\text{CW}}^{48}$	0.0329	0.0312	0.0321	0.0310	0.0291	0.0288
$\Delta r_{\text{np}}^{208}$	0.189	0.195	0.194	0.195	0.263	0.273
$\Delta r_{\text{np}}^{48}$	0.139	0.090	0.128	0.099	0.100	0.105
α_{D}^{208}	19.35	20.15	19.51	20.20	22.77	22.98
α_{D}^{48}	2.29	2.29	2.29	2.23	2.68	2.85

give a very large electric dipole polarizability α_{D} for ²⁰⁸Pb and ⁴⁸Ca, i.e., $\alpha_{\text{D}}^{208} = 22.77$ (22.98) fm³ and $\alpha_{\text{D}}^{48} = 2.68$ (2.85) fm³, much larger than the measured values of $\alpha_{\text{D}}^{208} = 19.6 \pm 0.6$ fm³ [69, 70] and $\alpha_{\text{D}}^{48} = 2.07 \pm 0.22$ fm³ [71] at RCNP. In addition, the predicted EOS of pure neutron matter (PNM) from (e)S500_T contradicts with the microscopic many-body theories [34]. Compared to the S500_T and eS500_T, the (extended) Skyrme EDF (e)S240_T with $b_{\text{IV}} = 240$ MeV · fm⁵ can simultaneously reproduce the measured α_{D} and ΔF_{CW} in ²⁰⁸Pb and ⁴⁸Ca within 1 σ error. Furthermore, the (e)S240_T predictions on the EOS for SNM and PNM agree well with the constraints from flow data in heavy-ion collisions [72] and microscopic many body theories [34], respectively. See Supplemental Material for the details.

The S240 and eS240 are constructed based on the standard and extended Skyrme interactions, respectively, with $b_{\text{IV}} = 240$ MeV · fm⁵ but turning off the tensor interactions (i.e., $\alpha_{\text{J}} = \beta_{\text{J}} = 0$) since usually they are not included in the Skyrme EDFs. It is interesting to mention that the S240 and eS240 have very similar performance in describing experimental data as the S240_T and eS240_T (see Supplemental Material), implying that the tensor interactions are not important for $b_{\text{IV}} = 240$ MeV · fm⁵. However, we note that the tensor interactions seem necessary to reasonably describe the spin-orbit splitting in typical doubly magic nuclei like ¹⁶O, ⁴⁸Ca and ²⁰⁸Pb for a very large b_{IV} as in (e)S500_T. We conclude that a strong IVSO coupling of $b_{\text{IV}} = 240$ MeV · fm⁵ can simultaneously reconcile the measured α_{D} and ΔF_{CW} in ²⁰⁸Pb and ⁴⁸Ca within 1 σ error.

To reveal the sensitivity of the $\Delta F_{\text{CW}}^{48}$ and $\Delta F_{\text{CW}}^{208}$ to the symmetry energy and the IVSO interaction, we carry out a correlation analysis based on eS240_T. By varying each model parameter with others fixed at their values in the eS240_T EDF, we calculate the $\Delta F_{\text{CW}}^{208}$ and $\Delta F_{\text{CW}}^{48}$, and the results are exhibited in Fig. 2. It is seen from Fig. 2 that the $\Delta F_{\text{CW}}^{208}$ is essentially only sensitive to L while the $\Delta F_{\text{CW}}^{48}$ is strongly correlated to both L and b_{IV} . The effects of all other parameters are relatively small. Similar correlations are observed for S240_T (see Fig. 5 in Supplemental Material).

The effects of the IVSO coupling b_{IV} can be understood via the spin-orbit contributions to the binding energy of a nucleus within the (extended) Skyrme EDF, i.e.,

$$E_{\text{so}} = \int d^3r \left[\frac{b_{\text{IS}}}{2} \mathbf{J} \cdot \nabla \rho + \frac{b_{\text{IV}}}{2} (\mathbf{J}_n - \mathbf{J}_p) \cdot \nabla (\rho_n - \rho_p) \right]. \quad (2)$$

For spherical nuclei like ⁴⁸Ca and ²⁰⁸Pb, the spin-orbit density \mathbf{J}_q only depends on the radius r , i.e., [51, 73]

$$J_q(r) = \frac{1}{4\pi r^3} \sum_i v_i^2 (2j_i + 1) \times \left[j_i(j_i + 1) - l_i(l_i + 1) - \frac{3}{4} \right] R_i^2(r), \quad (3)$$

where the sum runs over all (n, j, l) states having the same q , the v_i^2 is the occupation probability of each orbital, and $R_i(r)$ is the radial part of the wave function. From Eq. (3), one sees the orbital with $j_{>} = l + 1/2$ and its partner with $j_{<} = l - 1/2$ provide respectively positive and negative contributions to J_q . As a result, the J_q almost vanishes for the spin-saturated case, where all spin-orbit partners are either fully filled or empty, and the J_q might be large if only one of the spin-orbit partners is filled (and thus unpaired). For ²⁰⁸Pb, the J_p and J_n are dominated respectively by the unpaired $1h_{11/2}$ and $1i_{13/2}$ orbitals and they have roughly equal positive values, leading to small $J_n - J_p$ and thus negligible effects of b_{IV} on the $\Delta F_{\text{CW}}^{208}$. As to ⁴⁸Ca, all spin-orbit partners of

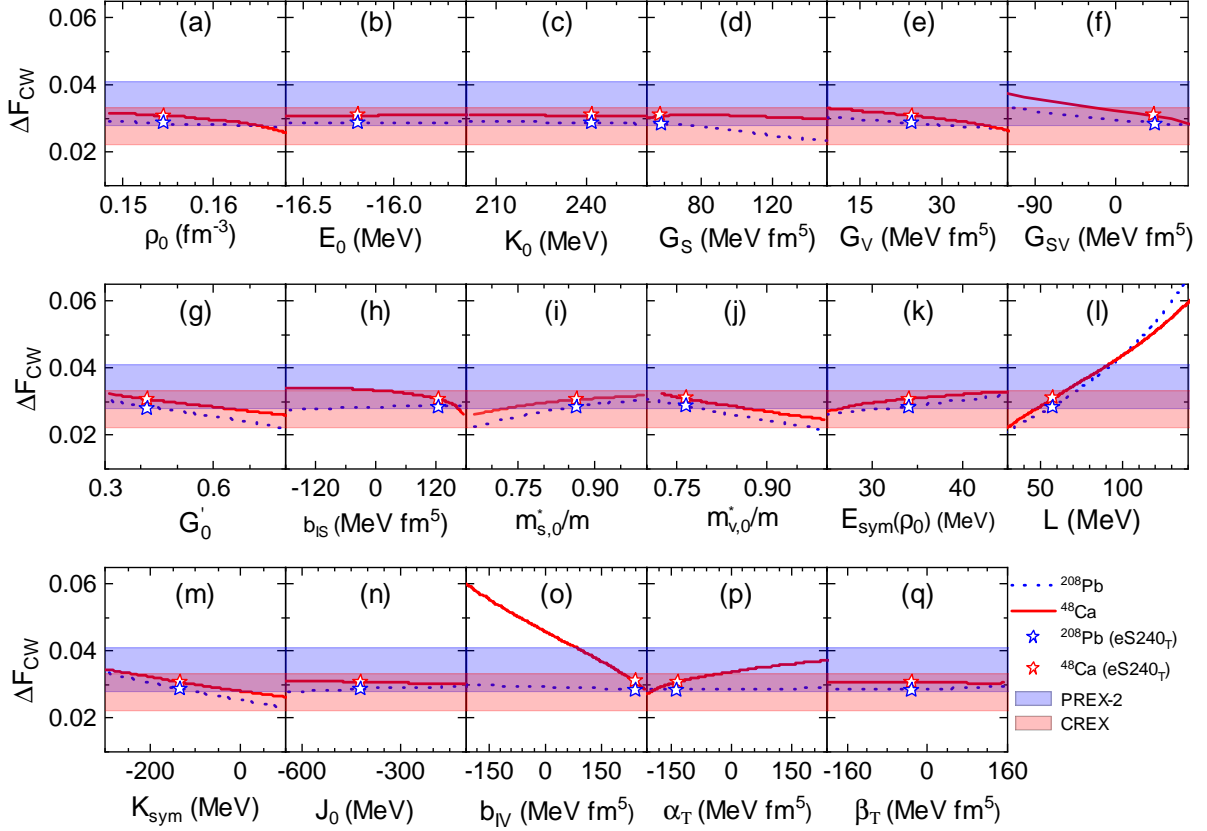


FIG. 2. The ΔF_{CW} in ^{208}Pb (blue dashed lines) and ^{48}Ca (red solid lines) obtained from eS240_T by varying individually ρ_0 (a), E_0 (b), K_0 (c), G_S (d), G_V (e), G_{SV} (f), G'_0 (g), b_{IS} (h), $m_{s,0}^*/m$ (i), $m_{v,0}^*/m$ (j), $E_{\text{sym}}(\rho_0)$ (k), L (l), K_{sym} (m), J_0 (n), b_{IV} (o), α_{T} (p) and β_{T} (q). The PREX-2 and CREX data with 1σ errors [2] are shown by the light blue and red bands, respectively. The eS240_T predictions are indicated by open stars.

protons are fully filled and thus J_p is very small, whereas the eight $1f_{7/2}$ neutrons are unpaired, leading to much larger J_n than J_p and thus strong effects from b_{IV} .

Given the strong positive $\Delta F_{\text{CW}}^{48(208)}-L$ correlation and the negative $\Delta F_{\text{CW}}^{48}-b_{\text{IV}}$ correlation as shown in Fig. 2, the PREX-CREX puzzle can be attributed to the small b_{IV} values in normal nuclear EDFs, which is roughly $40 \sim 80 \text{ MeV} \cdot \text{fm}^5$ in nonrelativistic Skyrme EDFs while it almost vanishes in standard RMF models. It is interesting to see in Fig. 1 that the nonrelativistic EDFs are systematically closer to the PREX-2 and CREX data compared to the relativistic ones, very likely due to the larger b_{IV} in the former. To simultaneously reproduce the PREX-2 and CREX data, one needs to take a larger L value preferred by the PREX-2 data, together with a larger b_{IV} value favored by the CREX data, and this is exactly the case for S500_T and eS500_T. However, since the $E_{\text{sym}}(\rho)$ around $2/3\rho_0$ is relatively well constrained by nuclear masses [14, 74, 75], such a large L would lead to rather small $E_{\text{sym}}(\rho)$ below $2/3\rho_0$, and thus too large electric dipole polarizability α_{D} , which is essentially determined by the $E_{\text{sym}}(\rho)$ around $\rho_0/3$ [76–78]. We find that to simultaneously reproduce the PREX-2 and CREX re-

sults together with the measured α_{D} in ^{208}Pb [69, 70] and ^{48}Ca [71] within 1σ error, L and b_{IV} should be around 55 MeV and $240 \text{ MeV} \cdot \text{fm}^5$, respectively, resulting in $\Delta r_{\text{np}}(^{208}\text{Pb}) \approx 0.19 \text{ fm}$ and $\Delta r_{\text{np}}(^{48}\text{Ca}) \approx 0.12 \text{ fm}$, as shown in Tab. I. We note $L \approx 55 \text{ MeV}$ nicely agrees with the world-averaged value [79, 80], and the $\Delta r_{\text{np}}(^{208}\text{Pb}) \approx 0.19 \text{ fm}$ and $\Delta r_{\text{np}}(^{48}\text{Ca}) \approx 0.12$ are also in good agreement with ab initio calculations [81, 82].

Compared to $b_{\text{IV}} \approx 40 \sim 80 \text{ MeV} \cdot \text{fm}^5$ in normal Skyrme EDFs, the six new EDFs constructed in the present work have much stronger IVSO interaction with b_{IV} larger than about four time of that in normal Skyrme EDFs, which is the key to reconcile the PREX-2 and CREX data. Within the RMF model, the strong IVSO coupling can be from isovector mesons and their exchange terms [62–66]. In addition, the SO interaction can be density dependent due to relativistic effects [62–66, 83] or the three-nucleon interactions [84]. These aspects are worthy of further study. Given the importance of SO coupling in nuclei, such a strong IVSO interaction is expected to have significant impacts on the properties of nuclei with unpaired neutrons or protons, and thus on many hot topics in nuclear physics, e.g., the location of

neutron dripline, the shell evolution and new magic numbers, the properties of superheavy nuclei, and so on.

Conclusions.—Within the Skyrme-like EDFs, we have demonstrated that the PREX-CREX puzzle can be solved by including a strong isovector spin-orbit interaction, which can significantly affect the ΔF_{CW} in ^{48}Ca but has essentially no effects on the ΔF_{CW} in ^{208}Pb . To reconcile the PREX-2 and CREX data, the strength of the isovector spin-orbit interaction should be larger than about four times of that in the conventional Skyrme-like EDFs. To further reconcile the measured electric dipole polarizabilities in ^{208}Pb and ^{48}Ca , we obtain $L \approx 55$ MeV, $\Delta r_{\text{np}}(^{208}\text{Pb}) \approx 0.19$ fm and $\Delta r_{\text{np}}(^{48}\text{Ca}) \approx 0.12$ fm. The strong isovector spin-orbit interaction suggested in our present work will have profound impacts on many topics in nuclear physics.

Our results suggest that while the ΔF_{CW} in stable closed-shell nuclei like ^{208}Pb and ^{60}Ni can uniquely constrain the density dependence of the symmetry energy near saturation density, the ΔF_{CW} in stable closed-shell nuclei with unpaired neutrons like ^{48}Ca and ^{90}Zr provides an ideal probe of the isovector spin-orbit interaction once the density behavior of the symmetry energy near saturation density is well constrained. It is thus interesting to measure the ΔF_{CW} of these nuclei in future parity-violation experiments, such as the Mainz Radius Experiment (MREX) [85, 86], which can help to determine the neutron skin, the symmetry energy and isovector spin-orbit interaction with minimal model dependence.

Acknowledgements.—This work was supported in part by the National Natural Science Foundation of China under Grant Nos. 12235010, 11905302 and 11625521, the National SKA Program of China No. 2020SKA0120300, and the Science and Technology Commission of Shanghai Municipality under Grant No. 23JC1402700.

* Corresponding author; zhangzh275@mail.sysu.edu.cn

† Corresponding author; lwchen@sjtu.edu.cn

- [1] D. Adhikari *et al.* (PREX), Accurate Determination of the Neutron Skin Thickness of ^{208}Pb through Parity-Violation in Electron Scattering, *Phys. Rev. Lett.* **126**, 172502 (2021).
- [2] D. Adhikari *et al.* (CREX), Precision Determination of the Neutral Weak Form Factor of Ca48, *Phys. Rev. Lett.* **129**, 042501 (2022).
- [3] M. Thiel, C. Sienti, J. Piekarewicz, C. J. Horowitz, and M. Vanderhaeghen, Neutron skins of atomic nuclei: per aspera ad astra, *J. Phys. G* **46**, 093003 (2019).
- [4] B. A. Brown, Neutron radii in nuclei and the neutron equation of state, *Phys. Rev. Lett.* **85**, 5296 (2000).
- [5] S. Typel and B. A. Brown, Neutron radii and the neutron equation of state in relativistic models, *Phys. Rev. C* **64**, 027302 (2001).
- [6] R. J. Furnstahl, Neutron radii in mean field models, *Nucl. Phys. A* **706**, 85 (2002).
- [7] S. Yoshida and H. Sagawa, Neutron skin thickness and equation of state in asymmetric nuclear matter, *Phys. Rev. C* **69**, 024318 (2004).
- [8] L.-W. Chen, C. M. Ko, and B.-A. Li, Nuclear matter symmetry energy and the neutron skin thickness of heavy nuclei, *Phys. Rev. C* **72**, 064309 (2005).
- [9] M. Centelles, X. Roca-Maza, X. Vinas, and M. Warda, Nuclear symmetry energy probed by neutron skin thickness of nuclei, *Phys. Rev. Lett.* **102**, 122502 (2009).
- [10] L.-W. Chen, C. M. Ko, B.-A. Li, and J. Xu, Density slope of the nuclear symmetry energy from the neutron skin thickness of heavy nuclei, *Phys. Rev. C* **82**, 024321 (2010).
- [11] P. G. Reinhard and W. Nazarewicz, Information content of a new observable: The case of the nuclear neutron skin, *Phys. Rev. C* **81**, 051303 (2010).
- [12] X. Roca-Maza, M. Centelles, X. Vinas, and M. Warda, Neutron skin of ^{208}Pb , nuclear symmetry energy, and the parity radius experiment, *Phys. Rev. Lett.* **106**, 252501 (2011).
- [13] B. K. Agrawal, J. N. De, and S. K. Samaddar, Determining the density content of symmetry energy and neutron skin: an empirical approach, *Phys. Rev. Lett.* **109**, 262501 (2012).
- [14] Z. Zhang and L.-W. Chen, Constraining the symmetry energy at subsaturation densities using isotope binding energy difference and neutron skin thickness, *Phys. Lett. B* **726**, 234 (2013).
- [15] C. Mondal, B. K. Agrawal, M. Centelles, G. Colò, X. Roca-Maza, N. Paar, X. Viñas, S. K. Singh, and S. K. Patra, Model dependence of the neutron-skin thickness on the symmetry energy, *Phys. Rev. C* **93**, 064303 (2016).
- [16] A. R. Raduta and F. Gulminelli, Nuclear skin and the curvature of the symmetry energy, *Phys. Rev. C* **97**, 064309 (2018).
- [17] W. G. Newton and G. Crocombe, Nuclear symmetry energy from neutron skins and pure neutron matter in a Bayesian framework, *Phys. Rev. C* **103**, 064323 (2021).
- [18] P.-G. Reinhard, X. Roca-Maza, and W. Nazarewicz, Information Content of the Parity-Violating Asymmetry in Pb208, *Phys. Rev. Lett.* **127**, 232501 (2021).
- [19] W. G. Lynch and M. B. Tsang, Decoding the density dependence of the nuclear symmetry energy, *Phys. Lett. B* **830**, 137098 (2022).
- [20] A. W. Steiner, M. Prakash, J. M. Lattimer, and P. J. Ellis, Isospin asymmetry in nuclei and neutron stars, *Phys. Rep.* **411**, 325 (2005).
- [21] V. Baran, M. Colonna, V. Greco, and M. Di Toro, Reaction dynamics with exotic nuclei, *Phys. Rep.* **410**, 335 (2005).
- [22] J. M. Lattimer and M. Prakash, Neutron Star Observations: Prognosis for Equation of State Constraints, *Phys. Rept.* **442**, 109 (2007).
- [23] B. A. Li, L. W. Chen, and C. M. Ko, Recent progress and new challenges in isospin physics with heavy-ion reactions, *Phys. Rep.* **464**, 113 (2008).
- [24] C. J. Horowitz, E. F. Brown, Y. Kim, W. G. Lynch, R. Michaels, A. Ono, J. Piekarewicz, M. B. Tsang, and H. H. Wolter, A way forward in the study of the symmetry energy: experiment, theory, and observation, *J. Phys. G* **41**, 093001 (2014).
- [25] S. Gandolfi, A. Gezerlis, and J. Carlson, Neutron Matter from Low to High Density, *Ann. Rev. Nucl. Part. Sci.* **65**, 303 (2015).

- [26] F. Özel and P. Freire, Masses, Radii, and the Equation of State of Neutron Stars, *Ann. Rev. Astron. Astrophys.* **54**, 401 (2016).
- [27] M. Baldo and G. F. Burgio, The nuclear symmetry energy, *Prog. Part. Nucl. Phys.* **91**, 203 (2016).
- [28] X. Roca-Maza and N. Paar, Nuclear equation of state from ground and collective excited state properties of nuclei, *Prog. Part. Nucl. Phys.* **101**, 96 (2018).
- [29] C. Drischler, J. W. Holt, and C. Wellenhofer, Chiral Effective Field Theory and the High-Density Nuclear Equation of State, *Ann. Rev. Nucl. Part. Sci.* **71**, 403 (2021).
- [30] B.-A. Li, B.-J. Cai, W.-J. Xie, and N.-B. Zhang, Progress in Constraining Nuclear Symmetry Energy Using Neutron Star Observables Since GW170817, *Universe* **7**, 182 (2021).
- [31] J. M. Mamei, C. J. Horowitz, J. Piekarewicz, B. Reed, and C. Sfienti, Neutron Skins: Weak Elastic Scattering and Neutron Stars [10.1146/annurev-nucl-102122-024207](https://arxiv.org/abs/10.1146/annurev-nucl-102122-024207) (2023).
- [32] P.-G. Reinhard, X. Roca-Maza, and W. Nazarewicz, Combined Theoretical Analysis of the Parity-Violating Asymmetry for Ca48 and Pb208, *Phys. Rev. Lett.* **129**, 232501 (2022).
- [33] E. Yüksel and N. Paar, Implications of parity-violating electron scattering experiments on 48Ca (CREX) and 208Pb (PREX-II) for nuclear energy density functionals, *Phys. Lett. B* **836**, 137622 (2023).
- [34] Z. Zhang and L.-W. Chen, Bayesian inference of the symmetry energy and the neutron skin in Ca48 and Pb208 from CREX and PREX-2, *Phys. Rev. C* **108**, 024317 (2023).
- [35] C. Mondal and F. Gulminelli, Nucleonic metamodeling in light of multimessenger, PREX-II, and CREX data, *Phys. Rev. C* **107**, 015801 (2023).
- [36] S. Tagami, T. Wakasa, and M. Yahiro, Slope parameters determined from CREX and PREX2 [10.48550/arXiv.2210.03313](https://arxiv.org/abs/10.48550/arXiv.2210.03313) (2022).
- [37] T. Miyatsu, M.-K. Cheoun, K. Kim, and K. Saito, Can the PREX-2 and CREX results be understood by relativistic mean-field models with the astrophysical constraints?, *Phys. Lett. B* **843**, 138013 (2023).
- [38] F. Sammarruca, The Neutron Skin of ^{48}Ca and ^{208}Pb : A Critical Analysis, *Symmetry* **16**, 34 (2024).
- [39] P. Papakonstantinou, Nuclear symmetry energy and the PREX-CREX neutron skin puzzle within the KIDS framework (2022) [arXiv:2210.02696 \[nucl-th\]](https://arxiv.org/abs/2210.02696).
- [40] M. Kumar, S. Kumar, V. Thakur, R. Kumar, B. K. Agrawal, and S. K. Dhiman, CREX- and PREX-II-motivated relativistic interactions and their implications for the bulk properties of nuclear matter and neutron stars, *Phys. Rev. C* **107**, 055801 (2023).
- [41] J. M. Lattimer, Constraints on Nuclear Symmetry Energy Parameters, *Particles* **6**, 30 (2023).
- [42] N. Liliani, A. M. Nugraha, J. P. Didingrum, and A. Sulaksono, Tensor and isovector–isoscalar terms of relativistic mean field model: Impacts on neutron-skin thickness, charge radius, and nuclear matter, *Nucl. Phys. A* **1042**, 122812 (2024).
- [43] B. T. Reed, F. J. Fattoyev, C. J. Horowitz, and J. Piekarewicz, Density dependence of the symmetry energy in the post-PREX-CREX era, *Phys. Rev. C* **109**, 035803 (2024).
- [44] M. Salinas and J. Piekarewicz, Impact of tensor couplings with scalar mixing on covariant energy density functionals, *Phys. Rev. C* **109**, 045807 (2024).
- [45] L. W. Chen, C. M. Ko, B. A. Li, and J. Xu, Density slope of the nuclear symmetry energy from the neutron skin thickness of heavy nuclei, *Phys. Rev. C* **82**, 024321 (2010).
- [46] C. J. Horowitz and J. Piekarewicz, Impact of spin-orbit currents on the electroweak skin of neutron-rich nuclei, *Phys. Rev. C* **86**, 045503 (2012).
- [47] M. G. Mayer, On closed shells in nuclei. 2, *Phys. Rev.* **75**, 1969 (1949).
- [48] O. Haxel, J. H. D. Jensen, and H. E. Suess, On the "Magic Numbers" in Nuclear Structure, *Phys. Rev.* **75**, 1766 (1949).
- [49] H.-P. Duerr, Relativistic Effects in Nuclear Forces, *Phys. Rev.* **103**, 469 (1956).
- [50] R. J. Furnstahl and B. D. Serot, Quantum hadrodynamics: Evolution and revolution, *Comments Nucl. Part. Phys.* **2**, A23 (2000).
- [51] D. Vautherin and D. M. Brink, Hartree-Fock calculations with Skyrme's interaction. 1. Spherical nuclei, *Phys. Rev. C* **5**, 626 (1972).
- [52] J. F. Berger, M. Girod, and D. Gogny, Microscopic analysis of collective dynamics in low energy fission, *Nucl. Phys. A* **428**, 23 (1984).
- [53] M. Bender, K. Rutz, P. G. Reinhard, J. A. Maruhn, and W. Greiner, Shell structure of superheavy nuclei in self-consistent mean field models, *Phys. Rev. C* **60**, 034304 (1999).
- [54] T. Lesinski, M. Bender, K. Bennaceur, T. Duguet, and J. Meyer, The Tensor part of the Skyrme energy density functional. I. Spherical nuclei, *Phys. Rev. C* **76**, 014312 (2007).
- [55] P. Klupfel, P. G. Reinhard, T. J. Burvenich, and J. A. Maruhn, Variations on a theme by Skyrme: A systematic study of adjustments of model parameters, *Phys. Rev. C* **79**, 034310 (2009).
- [56] E. Chabanat, J. Meyer, P. Bonche, R. Schaeffer, and P. Haensel, A Skyrme parametrization from subnuclear to neutron star densities, *Nucl. Phys. A* **627**, 710 (1997).
- [57] N. Chamel, S. Goriely, and J. M. Pearson, Further explorations of Skyrme-Hartree-Fock-Bogoliubov mass formulas. XI. Stabilizing neutron stars against a ferromagnetic collapse, *Phys. Rev. C* **80**, 065804 (2009).
- [58] L.-W. Chen and J.-Z. Gu, Correlations between the nuclear breathing mode energy and properties of asymmetric nuclear matter, *J. Phys. G* **39**, 035104 (2012).
- [59] M. Kortelainen, T. Lesinski, J. Moré, W. Nazarewicz, J. Sarich, N. Schunck, M. V. Stoitsov, and S. Wild, Nuclear energy density optimization, *Phys. Rev. C* **82**, 024313 (2010).
- [60] Z. Zhang and L.-W. Chen, Extended Skyrme interactions for nuclear matter, finite nuclei and neutron stars, *Phys. Rev. C* **94**, 064326 (2016).
- [61] F. Stancu, D. M. Brink, and H. Flocard, The tensor part of Skyrme's interaction, *Phys. Lett. B* **68**, 108 (1977).
- [62] M. M. Sharma, G. Lalazissis, J. König, and P. Ring, Isospin Dependence of the Spin-Orbit Force and Effective Nuclear Potentials, *Phys. Rev. Lett.* **74**, 3744 (1995).
- [63] P.-G. Reinhard and H. Flocard, Nuclear effective forces and isotope shifts, *Nuclear Physics A* **584**, 467488 (1995).
- [64] M. Bender, P.-H. Heenen, and P.-G. Reinhard, Self-consistent mean-field models for nuclear structure, *Rev. Mod. Phys.* **75**, 121 (2003).
- [65] A. Sulaksono, T. Burvenich, J. A. Maruhn, P. G. Rein-

- hard, and W. Greiner, The Nonrelativistic limit of the relativistic point coupling model, *Annals Phys.* **308**, 354 (2003).
- [66] J. P. Ebran, A. Mutschler, E. Khan, and D. Vretenar, Spin-orbit interaction in relativistic nuclear structure models, *Phys. Rev. C* **94**, 024304 (2016).
- [67] T.-G. Yue, L.-W. Chen, Z. Zhang, and Y. Zhou, Constraints on the Symmetry Energy from PREX-II in the Multimessenger Era, *Phys. Rev. Res.* **4**, L022054 (2022).
- [68] P. G. Reinhard, B. Schuetrumpf, and J. A. Maruhn, The Axial Hartree–Fock + BCS Code SkyAx, *Comput. Phys. Commun.* **258**, 107603 (2021).
- [69] A. Tamii, I. Poltoratska, P. Von Neumann-Cosel, Y. Fujita, T. Adachi, C. A. Bertulani, J. Carter, M. Dozono, H. Fujita, K. Fujita, K. Hatanaka, D. Ishikawa, M. Itoh, T. Kawabata, Y. Kalmykov, A. M. Krumbholz, E. Litvinova, H. Matsuura, K. Nakanishi, R. Neveling, H. Okamura, H. J. Ong, B. Özel-Tashenov, V. Y. Ponomarev, A. Richter, B. Rubio, H. Sakaguchi, Y. Sakemi, Y. Sasamoto, Y. Shimbara, Y. Shimizu, F. D. Smit, T. Suzuki, Y. Tameshige, J. Wambach, R. Yamada, M. Yosoi, and J. Zenihiro, Complete electric dipole response and the neutron skin in Pb208, *Phys. Rev. Lett.* **107**, 062502 (2011).
- [70] X. Roca-Maza, X. Viñas, M. Centelles, B. K. Agrawal, G. Colo', N. Paar, J. Piekarewicz, and D. Vretenar, The neutron skin thickness from the measured electric dipole polarizability in ^{68}Ni , ^{120}Sn , and ^{208}Pb , *Phys. Rev. C* **92**, 064304 (2015).
- [71] J. Birkhan *et al.*, Electric dipole polarizability of ^{48}Ca and implications for the neutron skin, *Phys. Rev. Lett.* **118**, 252501 (2017).
- [72] P. Danielewicz, R. Lacey, and W. G. Lynch, Determination of the equation of state of dense matter, *Science* **298**, 1592 (2002).
- [73] G. Colo', H. Sagawa, S. Fracasso, and P. F. Bortignon, Spin-orbit splitting and the tensor component of the Skyrme interaction, *Phys. Lett. B* **646**, 227 (2007), [Erratum: *Phys.Lett.B* 668, 457 (2008)].
- [74] B. A. Brown, Constraints on the skyrme equations of state from properties of doubly magic nuclei, *Phys. Rev. Lett.* **111**, 232502 (2013).
- [75] M. Qiu, B.-J. Cai, L.-W. Chen, C.-X. Yuan, and Z. Zhang, Bayesian model averaging for nuclear symmetry energy from effective proton-neutron chemical potential difference of neutron-rich nuclei, *Phys. Lett. B* **849**, 138435 (2024).
- [76] Z. Zhang and L.-W. Chen, Electric dipole polarizability in ^{208}Pb as a probe of the symmetry energy and neutron matter around $\rho_0/3$, *Phys. Rev. C* **92**, 031301 (2015).
- [77] J. Xu, J. Zhou, Z. Zhang, W.-J. Xie, and B.-A. Li, Constraining isovector nuclear interactions with giant resonances within a Bayesian approach, *Phys. Lett. B* **810**, 135820 (2020).
- [78] Z. Zhang, X.-B. Feng, and L.-W. Chen, Bayesian inference on isospin splitting of nucleon effective mass from giant resonances in ^{208}Pb , *Chin. Phys. C* **45**, 064104 (2021).
- [79] B. A. Li and X. Han, Constraining the neutron-proton effective mass splitting using empirical constraints on the density dependence of nuclear symmetry energy around normal density, *Phys. Lett. B* **727**, 276 (2013).
- [80] M. Oertel, M. Hempel, T. Klähn, and S. Typel, Equations of state for supernovae and compact stars, *Rev. Mod. Phys.* **89**, 015007 (2017).
- [81] G. Hagen *et al.*, Neutron and weak-charge distributions of the ^{48}Ca nucleus, *Nature Phys.* **12**, 186 (2015).
- [82] B. Hu *et al.*, Ab initio predictions link the neutron skin of ^{208}Pb to nuclear forces, *Nature Phys.* **18**, 1196 (2022).
- [83] J. M. Pearson and M. Farine, Relativistic mean-field theory and a density-dependent spin-orbit Skyrme force, *Phys. Rev. C* **50**, 185 (1994).
- [84] H. Nakada and T. Inakura, Effects of three-nucleon spin-orbit interaction on isotope shifts of Pb nuclei, *Phys. Rev. C* **91**, 021302 (2015).
- [85] D. Becker *et al.*, The P2 experiment, *Eur. Phys. J. A* **54**, 208 (2018).
- [86] S. Schlimme, K. Aulenbacher, S. Baunack, N. Berger, A. Denig, L. Doria, A. Khoukaz, H. Merkel, C. Sfienti, and M. Thiel, The MESA physics program, in *16th International Conference on Meson-Nucleon Physics and the Structure of the Nucleon* (2024) arXiv:2402.01027 [nucl-ex].
- [87] M. Wang, W. J. Huang, F. G. Kondev, G. Audi, and S. Naimi, The AME 2020 atomic mass evaluation (II). Tables, graphs and references, *Chin. Phys. C* **45**, 030003 (2021).
- [88] I. Angeli and K. P. Marinova, Table of experimental nuclear ground state charge radii: An update, *Atom. Data Nucl. Data Tabl.* **99**, 69 (2013).
- [89] F. Le Blanc *et al.*, Charge-radius change and nuclear moments in the heavy tin isotopes from laser spectroscopy: Charge radius of ^{132}Sn , *Phys. Rev. C* **72**, 034305 (2005).
- [90] V. I. Isakov, K. I. Erokhina, H. Mach, M. Sanchez-Vega, and B. Fogelberg, On the difference between proton and neutron spin orbit splittings in nuclei, *Eur. Phys. J. A* **14**, 29 (2002).
- [91] N. Schwierz, I. Wiedenhover, and A. Volya, Parameterization of the Woods-Saxon Potential for Shell-Model Calculations, (2007).

SUPPLEMENTAL MATERIAL

In this Supplemental Material, we provide details on (I) the Skyrme-like energy density functionals (EDFs) used in this work, (II) the calculation of the charge and weak form factors, (III) the performance of the six newly constructed Skyrme-like EDFs in the description of finite nuclei and nuclear matter, and (IV) correlation analysis of the charge-weak form factor difference in ^{48}Ca and ^{208}Pb based on the S240_T EDF.

I. EXTENDED SKYRME ENERGY DENSITY FUNCTIONAL WITH THE INCLUSION OF TENSOR FORCE

The conventional standard Skyrme interaction is given by (see, e.g., Ref. [56]):

$$v(\mathbf{r}_1, \mathbf{r}_2) = t_0(1 + x_0 P_\sigma) \delta(\mathbf{r}) + \frac{1}{2} t_1(1 + x_1 P_\sigma) [\mathbf{k}'^2 \delta(\mathbf{r}) + \delta(\mathbf{r}) \mathbf{k}^2] + t_2(1 + x_2 P_\sigma) \mathbf{k}' \cdot \delta(\mathbf{r}) \mathbf{k} + \frac{1}{6} t_3(1 + x_3 P_\sigma) [\rho(\mathbf{R})]^\alpha \delta(\mathbf{r}) + i W_0 (\boldsymbol{\sigma}_1 + \boldsymbol{\sigma}_2) \cdot [\mathbf{k}' \times \delta(\mathbf{r}) \mathbf{k}], \quad (4)$$

where $\mathbf{r} = \mathbf{r}_1 - \mathbf{r}_2$, $\mathbf{R} = \frac{1}{2}(\mathbf{r}_1 + \mathbf{r}_2)$, $\mathbf{k} = \frac{1}{2i}(\nabla_1 - \nabla_2)$ is the relative momentum with \mathbf{k}' being its conjugate acting on the left, the $\boldsymbol{\sigma}$ are Pauli spin operators, $P_\sigma = \frac{1}{2}(1 + \boldsymbol{\sigma}_1 \cdot \boldsymbol{\sigma}_2)$ is the spin exchange operator, and $\rho(\mathbf{R}) = \rho_n(\mathbf{R}) + \rho_p(\mathbf{R})$ is the total local density with ρ_n and ρ_p being neutron and proton densities, respectively. The $t_0 \sim t_3$ and $x_0 \sim x_3$ are the standard ‘‘Skyrme parameters’’, and W_0 is the spin-orbit coupling parameter. In this work, we also use the extended Skyrme interaction with the inclusion of additional effective momentum-dependent many-body force (see, e.g., Ref. [57]), that is

$$v' = v + \frac{1}{2} t_4(1 + x_4 P_\sigma) [\mathbf{k}'^2 \rho(\mathbf{R})^\beta \delta(\mathbf{r}) + \delta(\mathbf{r}) \rho(\mathbf{R})^\beta \mathbf{k}^2] + t_5(1 + x_5 P_\sigma) \mathbf{k}' \cdot \rho(\mathbf{R})^\gamma \delta(\mathbf{r}) \mathbf{k}. \quad (5)$$

Here the additional t_4 and t_5 terms are density-dependent generalization of the momentum-dependent t_1 and t_2 terms, then the extended Skyrme interaction has additional six parameters: t_4 , x_4 , t_5 , x_5 , β and γ . For the tensor force, we use the following zero-range form [61]

$$V_T = \frac{1}{2} T \left\{ \left[(\boldsymbol{\sigma}_1 \cdot \mathbf{k}') (\boldsymbol{\sigma}_2 \cdot \mathbf{k}') - \frac{1}{3} \mathbf{k}'^2 (\boldsymbol{\sigma}_1 \cdot \boldsymbol{\sigma}_2) \right] \delta(\mathbf{r}) + \delta(\mathbf{r}) \left[(\boldsymbol{\sigma}_1 \cdot \mathbf{k}) (\boldsymbol{\sigma}_2 \cdot \mathbf{k}) - \frac{1}{3} \mathbf{k}^2 (\boldsymbol{\sigma}_1 \cdot \boldsymbol{\sigma}_2) \right] \right\} + U \left\{ (\boldsymbol{\sigma}_1 \cdot \mathbf{k}') \delta(\mathbf{r}) (\boldsymbol{\sigma}_2 \cdot \mathbf{k}) - \frac{1}{3} (\boldsymbol{\sigma}_1 \cdot \boldsymbol{\sigma}_2) [\mathbf{k}' \cdot \delta(\mathbf{r}) \mathbf{k}] \right\}, \quad (6)$$

where T and U quantify the magnitude of the tensor force in states of even and odd relative motion, respectively.

Based on the extended Skyrme interaction with a zero-range tensor force, we can obtain the extended Skyrme potential energy density functional from Hartree-Fock calculation. For even-even nuclei, only time-even part of the Skyrme EDF contributes, and then the Skyrme EDF can be expressed in terms of local density ρ_q , kinetic-energy density τ_q and spin-current density \mathbf{J}_q of neutrons ($q = n$) and protons ($q = p$) defined by

$$\rho_q(\mathbf{r}) = \sum_i v_i^2 |\varphi_i(\mathbf{r})|^2, \quad (7)$$

$$\tau_q(\mathbf{r}) = \sum_i v_i^2 |\nabla \varphi_i(\mathbf{r})|^2, \quad (8)$$

$$\mathbf{J}_q(\mathbf{r}) = -i \sum_i v_i^2 \varphi_i^\dagger(\mathbf{r}) \nabla \times \hat{\sigma} \varphi_i(\mathbf{r}). \quad (9)$$

Here, φ_i is the single-particle wave function of state i , v_i is corresponding BCS occupation probability, and the sum runs over all states for the same given q . By further defining the isoscalar densities

$$\rho = \rho_n + \rho_p, \quad \tau = \tau_n + \tau_p, \quad \mathbf{J} = \mathbf{J}_n + \mathbf{J}_p,$$

and isovector densities

$$\tilde{\rho} = \rho_n - \rho_p, \quad \tilde{\tau} = \tau_n - \tau_p, \quad \tilde{\mathbf{J}} = \mathbf{J}_n - \mathbf{J}_p,$$

the Skyrme potential EDF without the Coulomb potential and pairing interaction can be expressed to be

$$\begin{aligned}
\mathcal{E}_{\text{Skyrme}} = & \frac{B_0 + B_3\rho^\alpha}{2}\rho^2 - \frac{B'_0 + B'_3\rho^\alpha}{2}\tilde{\rho}^2 + (B_1 + B_4\rho^\beta + B_5\rho^\gamma)\rho\tau - (B'_1 + B'_4\rho^\beta + B'_5\rho^\gamma)\tilde{\rho}\tilde{\tau} \\
& + \frac{2B_2 + (2\beta + 3)B_4\rho^\beta - B_5\rho^\gamma}{4}(\nabla\rho)^2 - \frac{2B'_2 + 3B'_4\rho^\beta - B'_5\rho^\gamma}{4}(\nabla\tilde{\rho})^2 - \frac{\beta B'_4}{2}\rho^{\beta-1}\tilde{\rho}\nabla\rho \cdot \nabla\tilde{\rho} \\
& + \frac{C_1 + C_2\rho^\beta + C_3\rho^\gamma}{2}\mathbf{J}^2 + \frac{C'_1 + C'_2\rho^\beta + C'_3\rho^\gamma}{2}\tilde{\mathbf{J}}^2 \\
& + \frac{b_{\text{IS}}}{2}\nabla\rho \cdot \mathbf{J} + \frac{b_{\text{IV}}}{2}\nabla\tilde{\rho} \cdot \tilde{\mathbf{J}} + \frac{\alpha_T + \beta_T}{4}\mathbf{J}^2 + \frac{\alpha_T - \beta_T}{4}\tilde{\mathbf{J}}^2.
\end{aligned} \tag{10}$$

Here, the coefficients B_i , B'_i , C_i and C'_i are uniquely related to the Skyrme parameters t_i and x_i by

$$\begin{aligned}
B_0 &= \frac{3}{4}t_0, & B'_0 &= \frac{1}{2}t_0\left(\frac{1}{2} + x_0\right), \\
B_1 &= \frac{3}{16}t_1 + \frac{5}{16}t_2 + \frac{1}{4}t_2x_2, & B'_1 &= \frac{1}{8}\left[t_1\left(\frac{1}{2} + x_1\right) - t_2\left(\frac{1}{2} + x_2\right)\right], \\
B_2 &= \frac{9}{32}t_1 - \frac{5}{32}t_2 - \frac{1}{8}t_2x_2, & B'_2 &= \frac{1}{16}\left[3t_1\left(\frac{1}{2} + x_1\right) + t_2\left(\frac{1}{2} + x_2\right)\right], \\
B_3 &= \frac{1}{8}t_3, & B'_3 &= \frac{1}{12}t_3\left(\frac{1}{2} + x_3\right), \\
B_4 &= \frac{3}{16}t_4, & B'_4 &= \frac{1}{8}t_4\left(\frac{1}{2} + x_4\right), \\
B_5 &= \frac{5}{16}t_5 + \frac{1}{4}t_5x_5, & B'_5 &= -\frac{1}{8}t_5\left(\frac{1}{2} + x_5\right), \\
C_1 &= \eta_{\text{tIs}}\frac{1}{8}\left[t_1\left(\frac{1}{2} - x_1\right) - t_2\left(\frac{1}{2} + x_2\right)\right], & C'_1 &= \eta_{\text{tIs}}\frac{1}{16}(t_1 - t_2), \\
C_2 &= \eta_{\text{tIs}}\frac{1}{8}t_4\left(\frac{1}{2} - x_4\right), & C'_2 &= \eta_{\text{tIs}}\frac{1}{16}t_4, \\
C_3 &= -\eta_{\text{tIs}}\frac{1}{8}t_5\left(\frac{1}{2} + x_5\right), & C'_3 &= -\eta_{\text{tIs}}\frac{1}{16}t_5.
\end{aligned} \tag{11}$$

Note that the tensor spin-orbit J_q^2 terms related to C_i and C'_i are omitted in many Skyrme EDFs. Therefore, we use the parameter η_{tIs} as a switch factor [55] where $\eta_{\text{tIs}} = 1$ and 0 represent the full inclusion and absence of the J_q^2 terms, respectively. The parameters b_{IS} and b_{IV} control the strength of spin-orbit interactions. For zero-range two-body spin-orbit interaction used in the (extended) Skyrme interaction one has $b_{\text{IS}} = 3b_{\text{IV}} = 3W_0/2$. In this work, we start from the energy density functional and consider them as free and independent parameters.

The nucleon mean field Hamiltonian is given by

$$\hat{h}_q = -\nabla \cdot \frac{\hbar^2}{2m_q^*}\nabla + U_q + i\mathbf{W}_q \cdot (\boldsymbol{\sigma} \times \nabla), \quad q = n, p, \tag{12}$$

where the single-nucleon fields can be derived from the energy density \mathcal{E} by

$$\frac{\hbar^2}{2m_q^*} = \frac{\partial\mathcal{E}}{\partial\tau_q}, \quad U_q = \frac{\partial\mathcal{E}}{\partial\rho_q} - \nabla \cdot \frac{\partial\mathcal{E}}{\partial[\nabla\rho_q]}, \quad \mathbf{W}_q = \frac{\partial\mathcal{E}}{\partial\mathbf{J}_q}. \tag{13}$$

From Eq. (10), one can obtain the nucleon effective mass m_q^* , i.e.,

$$\frac{\hbar^2}{2m_q^*} = \frac{\hbar^2}{2m} + (B_1 + B_4\rho^\beta + B_5\rho^\gamma)\rho - t_q(B'_1 + B'_4\rho^\beta + B'_5\rho^\gamma)\tilde{\rho}, \tag{14}$$

the single nucleon potential (without Coulomb potential)

$$\begin{aligned}
U_q = & B_0\rho - t_q B'_0\tilde{\rho} + B_1\tau - t_q B'_1\tilde{\tau} + \frac{\alpha + 2}{2}B_3\rho^{\alpha+1} - \frac{B'_3}{2}(\alpha\tilde{\rho} + 2t_q\rho)\rho^{\alpha-1}\tilde{\rho} \\
& + (\beta + 1)B_4\rho^\beta\tau + (\gamma + 1)B_5\rho^\gamma\tau - (B'_4\beta\rho^\beta + B'_5\gamma\rho^\gamma)\tilde{\rho}\tilde{\tau} - t_q(B'_1 + B'_4\rho^\beta + B'_5\rho^\gamma)\tilde{\tau} \\
& - \frac{\beta(2\beta + 3)B_4\rho^{\beta-1} - B_5\gamma\rho^{\gamma-1}}{4}(\nabla\rho)^2 - \frac{2B_2 + (2\beta + 3)B_4\rho^\beta - B_5\rho^\gamma}{2}\nabla^2\rho \\
& - \frac{3\beta B'_4\rho^{\beta-1} - \gamma B'_5\rho^{\gamma-1}}{4}\nabla\tilde{\rho} \cdot (2t_q\nabla\rho + \nabla\tilde{\rho}) - \frac{2B'_2 + 3B'_4\rho^\beta - B'_5\rho^\gamma}{2}t_q\nabla^2\tilde{\rho} \\
& + \frac{\beta B'_4}{2}\rho^{\beta-1}(\nabla\tilde{\rho})^2 + \frac{\beta B'_4}{2}\rho^{\beta-1}\tilde{\rho}\nabla^2\tilde{\rho} + \frac{\beta(\beta-1)B'_4}{2}\rho^{\beta-2}\tilde{\rho}(\nabla\rho)^2t_q + \frac{\beta B'_4}{2}\rho^{\beta-1}\tilde{\rho}(\nabla^2\rho)t_q \\
& + \frac{\beta C'_2\rho^{\beta-1} + \gamma C'_3\rho^{\gamma-1}}{2}\mathbf{J}^2 + \frac{\beta C'_2\rho^{\beta-1} + \gamma C'_3\rho^{\gamma-1}}{2}\mathbf{J}^2 - \frac{b_{\text{IS}}}{2}\nabla \cdot \mathbf{J} - t_q\frac{b_{\text{IV}}}{2}\nabla \cdot \tilde{\mathbf{J}}, \tag{15}
\end{aligned}$$

and the spin-orbit potential

$$\mathbf{W}_q = \frac{b_{\text{IS}}}{2}\nabla\rho + t_q\frac{b_{\text{IV}}}{2}\nabla(\rho_n - \rho_p) + \frac{\alpha_J + \beta_J}{2}\mathbf{J} + t_q\frac{\alpha_J - \beta_J}{2}(\mathbf{J}_n - \mathbf{J}_p), \tag{16}$$

where $t_q = 1$ and -1 for $q = n$ and p , respectively. The parameters α_J and β_J in the spin-orbit potentials are defined by

$$\alpha_J = \alpha_C + \alpha_T, \quad \beta_J = \beta_C + \beta_T,$$

with the tensor-parameters α_T and β_T given by

$$\alpha_T = \frac{5}{12}U, \quad \beta_T = \frac{5}{24}(T + U), \tag{17}$$

and the central-exchange parameters given by

$$\alpha_C = 2C_1 + 2C_2\rho^\beta + 2C_3\rho^\gamma, \quad \beta_C = 2C'_1 + 2C'_2\rho^\beta + 2C'_3\rho^\gamma. \tag{18}$$

For a given parameter sets of ($t_0 \sim t_5$, $x_0 \sim x_5$, α , β , γ , b_{IS} , b_{IV} , α_T and β_T), the ground-state properties of a nucleus can be obtained from Hartree-Fock calculations based on the nuclear mean field Hamiltonian (12). For simplicity, we fix $\beta = \gamma = 1$ in this work. The detailed parameter values for the six newly constructed Skyme-like EDFs are listed in Table 1 of the main paper, and those for the coefficients B_i and C_i [see Eq. (11)] are listed in Table II.

II. CHARGE AND WEAK FORM FACTORS

The normalized nuclear form factors $F_C(q)$ and $F_W(q)$ are calculated by folding the nucleon form factor $F_t(q)$ ($t = n, p$) and the spin-orbit current form factor ($F_t^{(ls)}$) with the intrinsic nucleon electromagnetic form factor $G_{E/M,t}$ and weak form factor $G_{E/M,t}^{(W)}$ by [18]

$$F_C(q) = \frac{1}{Z} \sum_{t=p,n} \left[G_{E,t}(q)F_t(q) + G_{M,t}(q)F_t^{(ls)}(q) \right], \tag{19}$$

$$F_W(q) = \sum_{t=p,n} \frac{\left[G_{E,t}^{(W)}(q)F_t(q) + G_{M,t}^{(W)}(q)F_t^{(ls)}(q) \right]}{ZQ_p^{(W)} + NQ_n^{(W)}}, \tag{20}$$

where $N(Z)$ is the neutron(proton) number, and $Q_p^{(W)} = 0.0713$ and $Q_n^{(W)} = -0.9888$ are proton and neutron weak charges, respectively. The $G_{E/M,t}$ are derived from the isospin-coupled Sachs form factors, the relativistic Darwin correction has been included and the center-of-mass corrections are taken into account by simply renormalizing the nucleon mass m_N to $(1 - 1/A)m_N$ in the HF calculation (see, e.g., Ref. [64] for details). The weak intrinsic nucleon form factors $G_{E/M,t}^{(W)}$ are then determined by [18]

$$\begin{aligned}
G_{E/M,n}^{(W)} &= Q_n^{(W)}G_{E/M,p} + Q_p^{(W)}G_{E/M,n} + Q_n^{(W)}G_{E/M,s}, \\
G_{E/M,p}^{(W)} &= Q_p^{(W)}G_{E/M,p} + Q_n^{(W)}G_{E/M,n} + Q_n^{(W)}G_{E/M,s},
\end{aligned} \tag{21}$$

TABLE II. Values of B_i and C_i coefficients (see Eq.(11)) for the 6 new EDFs, i.e., S240, eS240, S240_T, eS240_T, S500_T and eS500_T.

Quantity	S240	eS240	S240 _T	eS240 _T	S500 _T	eS500 _T
B_0 (MeV · fm ³)	-1522.01	-1332.95	-1509.93		-1457.18	-1224.51
B'_0 (MeV · fm ³)	-776.750	-773.665	-785.960	-689.517	-2.68690	-301.036
B_1 (MeV · fm ⁵)	2.2644	12.2077	0.915374	24.9883	-2.77971	19.5659
B'_1 (MeV · fm ⁵)	6.5935	-0.38529	1.53454	5.67033	61.8550	40.1165
B_2 (MeV · fm ⁵)	118.856	194.501	116.638	203.554	117.790	194.804
B'_2 (MeV · fm ⁵)	-70.2871	-37.6588	-24.7165	-53.1573	-32.2209	166.682
B_3 (MeV · fm ^{3+3α})	1714.23	1610.31	1706.60	1513.37	1697.44	1600.97
B'_3 (MeV · fm ^{3+3α})	690.006	920.361	748.525	724.393	-1094.24	-495.702
B_4 (MeV · fm ^{5+3β})	0	-301.590	0	-322.124	0	-340.371
B'_4 (MeV · fm ^{5+3β})	0	232.462	0	274.673	0	-498.017
B_5 (MeV · fm ^{5+3β})	0	278.281	0	295.959	0	288.309
B'_5 (MeV · fm ^{5+3β})	0	-325.079	0	-328.159	0	580.922
C_1 (MeV · fm ⁵)	113.580	104.334	64.5157	128.008	101.948	-78.4280
C'_1 (MeV · fm ⁵)	-0.526945	36.2206	20.2351	27.9500	-18.4053	93.2463
C_2 (MeV · fm ^{5+3β})	0	-433.522	0	-489.422	0	271.103
C'_2 (MeV · fm ^{5+3β})	0	-100.530	0	-107.375	0	-113.457
C_3 (MeV · fm ^{5+3β})	0	-325.079	0	-328.159	0	580.922
C'_3 (MeV · fm ^{5+3β})	0	123.959	0	120.120	0	483.384
b_{IS} (MeV · fm ⁵)	160.806	149.723	123.178	124.779	100.560	118.870
b_{IV} (MeV · fm ⁵)	240.000	240.000	240.000	240.000	500.000	500.000
α_T (MeV · fm ⁵)	0	0	-200.163	-132.004	-121.47	-1.6178
β_T (MeV · fm ⁵)	0	0	-51.2445	-32.56077	-295.74	-244.841

with the strange-quark electromagnetic form factors $G_{E/M,s}$ given by

$$G_{E,s}(q) = \rho_s \frac{\hbar^2 q^2 / (4c^2 m_N^2)}{1 + 4.97 \hbar^2 q^2 / (4c^2 m_N^2)}, \quad (22)$$

$$G_{M,s}(q) = \kappa_s \frac{\hbar^2}{(4c^2 m_N^2)}.$$

The strange quark electric coupling ρ_s and the strange quark magnetic moment κ_s are respectively taken to be -0.24 and -0.017 [18].

III. PERFORMANCE OF THE SIX NEW SKYRME-LIKE EDFS IN THE DESCRIPTION OF FINITE NUCLEI AND NUCLEAR MATTER

Figure 3 shows the relative deviations of the binding energies and charge radii for ¹⁶O, ⁴⁰Ca, ⁴⁸Ca, ⁵⁶Ni, ⁶⁸Ni, ⁸⁸Sr, ⁹⁰Zr, ¹⁰⁰Sn, ¹³²Sn, and ²⁰⁸Pb calculated with the six new EDFs from the corresponding experimental data [55, 87–89]. The shaded bands indicate a deviation with $\pm 1\%$. It is seen that all the six EDFs well reproduce the ground-state binding energies and charge radii of the ten typical (semi-)closed-shell spherical nuclei, with relative deviations less than 1%, except for the light nucleus ¹⁶O, for which the mean field models are relatively less valid.

We further present in Fig. 4 the relative deviations of the spin-orbit splittings of some typical orbitals in several doubly magic nuclei ¹⁶O, ⁴⁰Ca, ⁴⁸Ca, ⁵⁶Ni, ¹³²Sn and ²⁰⁸Pb predicted by the six new EDFs from the experimental data [90, 91]. As can be seen from Fig. 4, all the six new EDFs can reproduce overall the spin-orbit splittings of the chosen doubly magic nuclei within $\pm 50\%$ relative deviations, except that the S500_T EDF overestimates the proton $2d_{3/2} - 2d_{5/2}$ splitting in ¹³²Sn by about 80% relative error. Remarkably, although the strength parameter for the isovector spin-orbit interaction in the S500_T and eS500_T is about ten times larger than that of normal Skyrme EDFs, they can still reasonably describe the spin-orbit splittings in typical doubly magic nuclei with the inclusion of tensor force, compared to some typical conventional Skyrme interactions (see, e.g., Fig. 9 in Ref. [64]).

Figure 5 (a) and (b) show respectively the pressure P_{SNM} in symmetric nuclear matter and the energy per neutron E_{PNM} in pure neutron matter as functions of nucleon density ρ predicted by the six EDFs. For comparison, the constrains on P_{SNM} from flow data in heavy ion collisions [72] and the predictions from microscopic many-body

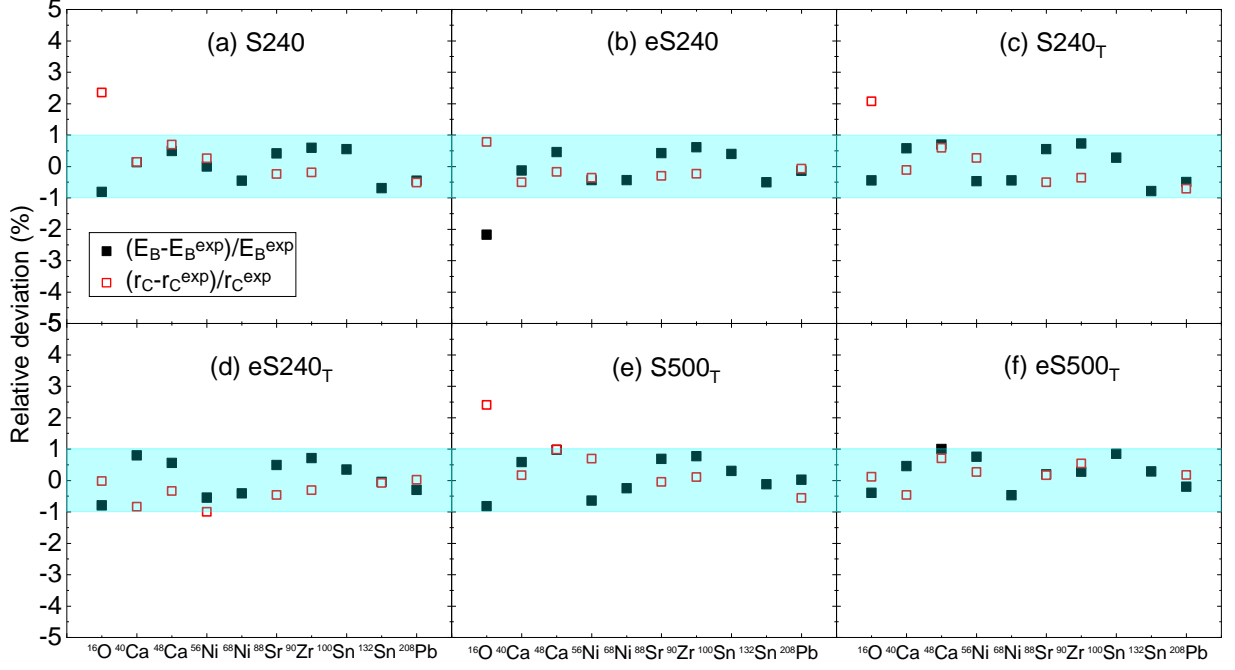


FIG. 3. Relative deviation of the binding energies E_B and charge radii r_c of ^{16}O , ^{40}Ca , ^{48}Ca , ^{56}Ni , ^{68}Ni , ^{88}Sr , ^{90}Zr , ^{100}Sn , ^{132}Sn , ^{144}Sm , and ^{208}Pb obtained using the S240 (a), eS240 (b), S240_T (c), eS240_T (d), S500_T (e) and eS500_T (f) from the experimental measurements [55, 87–89]. The shaded region indicates $\pm 1\%$ relative deviation.

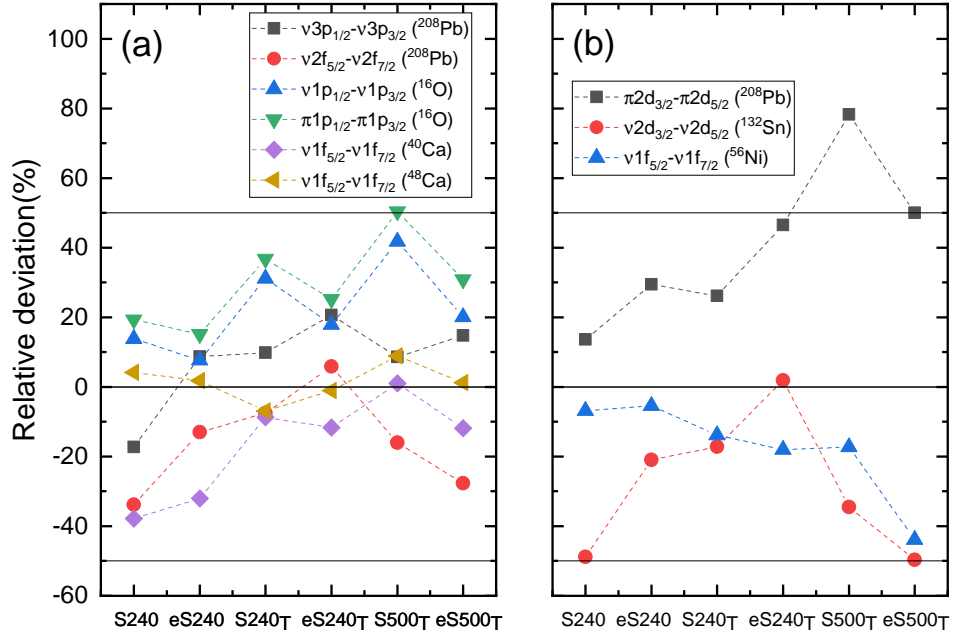


FIG. 4. Same as Fig. 3 but for the spin-orbit splittings of some typical orbitals in ^{16}O , ^{40}Ca , ^{48}Ca , ^{56}Ni , ^{132}Sn and ^{208}Pb .

theories [34] are shown as shadowed regions in panels (a) and (b), respectively. One sees that all the six EDFs agree with the flow data constraints on the P_{SNM} . In addition, while the four EDFs S240, eS240, S240_T, eS240_T can nicely describe the $E_{\text{PNM}}(\rho)$ of microscopic many-body theories, the $E_{\text{PNM}}(\rho)$ from the S500_T and eS500_T significantly deviate from the predictions of microscopic many-body theories due to their too stiff symmetry energy.

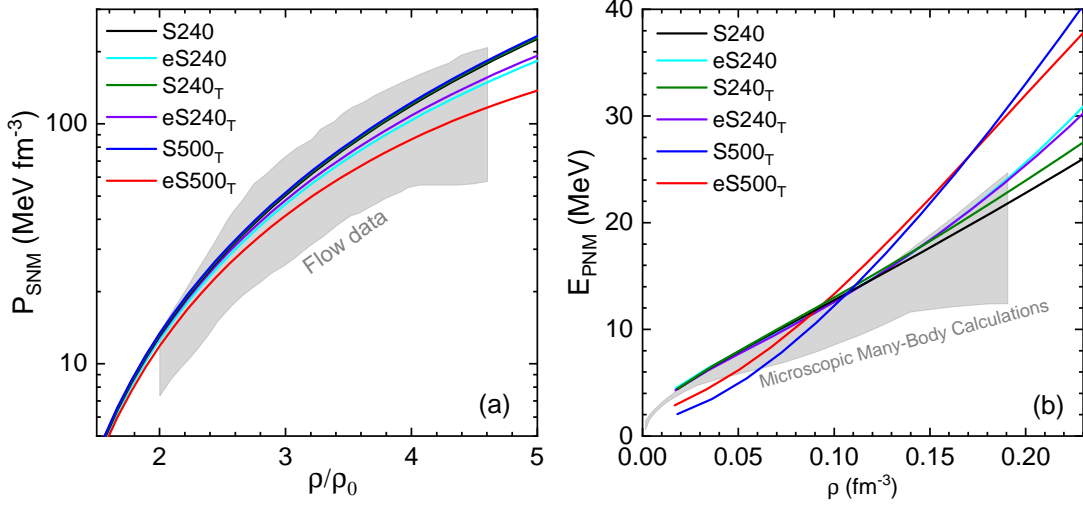


FIG. 5. Pressure $P_{\text{SNM}}(\rho)$ in symmetric nuclear matter (a) and the energy per neutron $E_{\text{PNM}}(\rho)$ for pure neutron matter (b) as functions of nucleon density ρ predicted by the six new Skyrme-like EDFs, i.e., S240, eS240, S240_T, eS240_T, S500_T and eS500_T. For comparison, the constraints on the $P_{\text{SNM}}(\rho)$ from flow data in heavy ion collisions [72] and the predictions from microscopic many-body theories [34] are also shown as shadowed regions in panels (a) and (b), respectively.

IV. CORRELATION OF THE CHARGE-WEAK FORM FACTOR DIFFERENCE

Similar to Figure 2 in the main paper, we show in Fig. 6 the charge-weak form factor difference ΔF_{CW} in ^{48}Ca and ^{208}Pb with the S240_T by varying each model parameter individually. It is seen that, the $\Delta F_{\text{CW}}^{208}$ is essentially only sensitive to the density slope parameter L of the symmetry energy, while the $\Delta F_{\text{CW}}^{48}$ exhibits strong positive and negative correlations with the L and b_{IV} , respectively. All other parameters have minor effects on the $\Delta F_{\text{CW}}^{48}$ and $\Delta F_{\text{CW}}^{208}$. The results of correlation analysis based on the S240_T EDF are consistent with those based on the eS240_T.

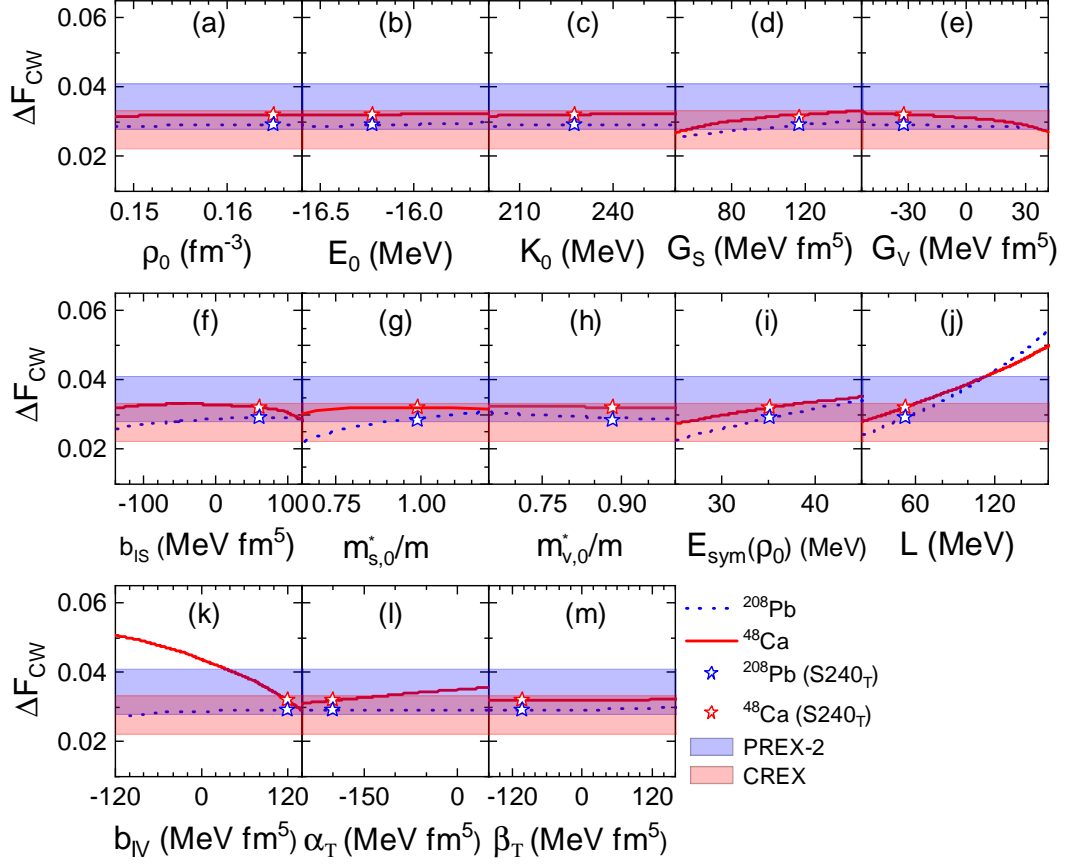


FIG. 6. The ΔF_{CW} in ^{208}Pb (dashed lines) and ^{48}Ca (solid lines) from the S240_T EDF by varying individually ρ_0 (a), E_0 (b), K_0 (c), G_S (d), G_V (e), b_{IS} (f), $m_{s,0}^*/m$ (g), $m_{v,0}^*/m$ (h), $E_{sym}(\rho_0)$ (i), L (j), b_{IV} (k), α_T (l) and β_T (m). The PREX-2 and CREX measurements with 1σ error are shown by the light blue and red bands, respectively. The S240_T predictions are indicated by open stars.